Materials Physics and Mechanics 44 (2020) 348-365 Received: May 5, 2020

MODELING OF STATIC RECRYSTALLIZATION IN COMPLEXLY ALLOYED AUSTENITE

A.A. Vasilyev[1*], S.F. Sokolov[2], D.F. Sokolov[2], N.G. Kolbasnikov[1]

[1]Peter the Great St. Petersburg Polytechnic University, Polytekhnicheskaya, 29

195251, St. Petersburg, Russia

[2]PJSC Severstal, Mira, 30, 162608, Cherepovets, Russia

*e-mail: vasilyev_aa@mail.ru

Abstract. To predict the kinetics of static recrystallization and the resulting grain size in austenite of alloyed steels including additions of Nb, V, and Ti, a quantitative model is developed. Physically motivated, the model relates the activation energy of the process with that of bulk self-diffusion. The known dependence of the latter on the chemical composition of austenite solid solution, established previously, essentially simplifies the modeling. Employed empirical parameters have been fitted to relevant data covering a wide range of chemical compositions (23 steels) and sizes of recrystallized austenite grains. The model satisfactorily complies with experiments on steels whose apparent activation energy of recrystallization varies from 146.1 to 308.1 kJ/mol. It is notable as well that this performance has been achieved with no direct allowance for the pinning of grain boundaries by solute atoms (solute drag effect).

Keywords: steels, austenite, recrystallization, recovery, precipitation, carbonitrides, kinetics, modeling

1. Introduction

An important effect of static recrystallization on the austenite structure of hot rolled steels [1-20] and hence on their final (transformed) structure attracts a persisting practical interest. To simulate this phenomenon, the Kolmogorov-Johnson-Mehl-Avrami (KJMA) equation [21] is widely applied. Predictions by related models [2,3,11,19] satisfactorily comply with experiments at high temperatures in a wide range of chemical compositions where all alloying elements are completely dissolved in austenite. At the same time, the KJMA equation hardly enables allowance for the recovery phenomenon that precedes and accompanies the recrystallization and thus consumes its driving force. Besides, the deformation-induced precipitation of carbonitrides/carbides of microalloying elements (MAE) and their effect on the considered process kinetics are even harder to describe within the framework of KJMA. Several attempts [12,13,15] have been undertaken to formulate physically based models simultaneously involving the recovery, recrystallization, and deformation-induced precipitation in austenite. Although promising results are achieved in this way, quantitative models of this type should be refined in order to predict the effect of chemical composition on recrystallization kinetics in austenite of complexly alloyed steels including those which contain MAE.

To model the kinetics of recrystallization, activation energy of this process should be determined first. According to the physics of diffusional lattice rearrangements at moving boundaries of recrystallized grains, this energy should be comparable to that of grain boundary self-diffusion. The latter parameter, in turn, correlates with the energy of bulk self-diffusion

http://dx.doi.org/10.18720/MPM.4432020_7

(AESD). It is notable that experimental results obtained by the radioactive tracer technique, which have been compiled by the authors [22], indicate that AESD in solid solutions of austenite depends on their chemical composition. An empirical expression proposed in the last quoted paper enables accurate calculation of AESD in terms of quantities of alloying elements (C, Mn, Si, Ni, Cr, Mo, Nb, V, Ti) most important for up-to-date steels. It is shown that Mn, Si, Mo, Nb, Ti notably increase this energy whereas the latter is strongly reduced by C and, to a lesser degree, by Ni, Cr and V. With allowance for the physically motivated correlation between AESD and the activation energy of recrystallization, we will presume proportionality of these parameters where the former depends on the chemical composition of the steel. This presumption has been previously verified [23] by successful modeling of the normal grain growth in austenite of complexly alloyed steels.

The present paper formulates an integral model allowing for the three interacting processes: recrystallization, recovery, and deformation-induced precipitations. Empirical parameters of the model have been fitted to literature data as well as our experimental data on austenite recrystallization kinetics in steels of various compositions including those containing MAE.

2. Model description

The model quantitatively treats the main interrelated processes which form the structure of austenite in its hot deformation (recrystallization, recovery, precipitations on dislocations of deformed austenite). Some simplifying assumptions for involved microscopic mechanisms are made as follows.

Recrystallization simultaneously starts at embryos situated over grain boundaries of deformed austenite [12,13]. Alternative nucleation sites [24] (in-grain precipitates or dislocation substructure) are not considered. Carbonitrides Me(C,N) with Nb or V for Me, as well as carbides of Ti precipitate at nodal points of a uniform dislocation network [12,13,25]. Embryonic and growing precipitate particles keep a spherical shape whereas the critical nucleus radius keeps the same over the whole material. Therefore, uniformity of its chemical composition is assumed.

In the considered temperature range diffusion mobility of substitution atoms of alloying elements (Me) is significantly lower than that of C and N. That is why kinetics of the particle nucleation and growth is controlled by the diffusion rate of Me.

Recrystallization. We determine first the so-called extended recrystallized volume $X_{ext}(t)$ [21]:

$$X_{ext}(t) = N_{rex}\frac{4\pi}{3}\bar{R}^3_{rex}(t), \tag{1}$$

where N_{rex} is the volume density of nuclei and $\bar{R}_{rex}(t)$ is the average radius of new grains in time *t* after they were nucleated. To evaluate the velocity $V_G^{rex}(t)$ of their moving boundaries, the following expression is used:

$$V_G^{rex}(t) = M_{GB}^{rex}\,P_{rex}(t), \tag{2}$$

where $M_{GB}^{rex} \equiv M_{GB}^{rex}(T, Y_{AE})$ specifies mobility, T is absolute temperature and $Y_{AE} = \{y_C, y_{Mn}, y_{Si}, ...\}$ represents a set of average fractions of the sites of substitution and interstitial sublattices occupied, respectively, by the atoms of substitution alloying elements and carbon. The term $P_{rex}(t)$ in Eq. (2) expresses the driving pressure (force) of recrystallization. With Eq. (1) kept in mind and the form-factor of the order of unity included in N_{rex}, the extended recrystallized volume takes on form:

$$X_{ext}(t) = N_{rex}\left(\int_0^t M_{GB}^{rex} P_{rex}(\tau)\, d\tau\right)^3. \quad (3)$$

The actual recrystallized volume fraction $X(t)$ is expressed in terms of $X_{ext}(t)$ as follows [21]:

$$X(t) = 1 - \exp\left(-X_{ext}(t)\right). \quad (4)$$

Driving pressure of recrystallization. Such a pressure characterizes specific energy, accumulated in the deformed austenite; the main part of this quantity is due to the increased dislocation density [21]. An appropriate estimate for the driving pressure is:

$$P_{rex}(t) \cong 0.5\mu b^2 \rho_d(t), \quad (5)$$

where $\rho_d(t)$ is the dislocation density, μ is the shear modulus, $b = a_\gamma\sqrt{2}/2$ is the Burgers vector magnitude, and $a_\gamma = 0.364$ nm is the lattice parameter of austenite. This expression suggests energy of $0.5\mu b^2$ per unit length of dislocation.

The distribution of dislocations in constitutive grains of a deformed polycrystal is generally non-uniform [21]. Specifically, their density near grain boundaries significantly exceeds that in grain cores. Accordingly, for the dislocation density in Eq. (5) we have:

$$\rho_d(t) = \alpha_{d1}\overline{\rho}_d(t)\left(1 + \alpha_{d1}^{-1}\exp\left(-\alpha_{d2}X(t)\right)\right), \quad (6)$$

where $\overline{\rho}_d(t)$ is the average dislocation density calculated with allowance for recovery, and $\alpha_{d1}, \alpha_{d2} > 0$ are empirical parameters.

Based on the conventional treatment of the dislocation contribution to work hardening, calculated here with allowance for recovery (see Eqs. (16)-(18)), we use the expression:

$$\overline{\rho}_d(t) = \left(\frac{\Delta\sigma(t)}{\alpha_\rho M \mu b}\right)^2 \quad (7)$$

with the Taylor factor $M = 3.1$ and $\alpha_\rho \simeq 0.15$. The temperature dependence of the shear modulus is here evaluated according to [13]:

$$\mu \equiv \mu(T) = 8.1\times10^{10}\left[0.91 - \frac{T-300}{1810}\right] \text{(Pa)}. \quad (8)$$

Carbonitrides/carbides of MAE precipitated on dislocations of deformed austenite retard migration of grain boundaries (Zener's pinning) and hence reduce the effective driving pressure $P_{rex}^*(t)$:

$$P_{rex}^*(t) = P_{rex}(t) - P_Z(t), \quad (9)$$

where $P_Z(t)$ is Zener's pressure. The latter is expressed as:

$$P_Z(t) = 3\gamma_{GB}\sum_i \frac{f_p^i(t)}{\overline{R}_p^i(t)}, \quad (10)$$

where $f_p^i(t)$ is the volume fraction for particles of *i*-th type, $\overline{R}_p^i(t)$ is their average radius, γ_{GB} is the specific energy of recrystallized grain boundaries (empirical parameter).

Volume density of recrystallized grain nuclei. As noted above, the model assumes the nucleation of recrystallized grains at the initial grain boundaries of austenite. Thus, according to [13], the volume density of such nuclei takes on form:

$$N_{rex} = \frac{\alpha_{rex} S_{GB}}{S_c}, \quad (11)$$

where S_{GB} is the specific area of austenite grain boundaries, S_c is a boundary area occupied by one critical nucleus, α_{rex} is a geometrical parameter. Following [13], we will consider the area of the critical nucleus $S_c \sim P_{rex}^{-2}(t=0)$. Therefore, since the area of grain boundaries is inversely proportional to the grain size, Eq. (11) is reduced to:

$$N_{rex} = \frac{\alpha_{rex}^{*} P_{rex}^{2}(t=0)}{D_{\gamma 0}}, \tag{12}$$

where $D_{\gamma 0}$ is the average diameter of initial austenite grains and α_{rex}^{*} is an empirical parameter. With α_{rex}^{*} including the geometrical factor of the order of unity in Eq. (11), we estimate the average grain size in the recrystallized structure as follows:

$$D_{rex} = N_{rex}^{-1/3}. \tag{13}$$

Mobility of grain boundaries. When considering recrystallized grains, mobility of their boundaries is treated like that in the normal grain growth [23]:

$$M_{GB}^{rex}\left(T; Y_{AE}\right) = M_0^{rex} \exp\left(\frac{S_{GG}^{rex}(Y_{AE})}{R_g}\right) \exp\left(-\frac{Q_{GG}^{rex}(Y_{AE})}{R_g T}\right), \tag{14}$$

where $Q_{GG}^{rex}(Y_{AE})$ and $S_{GG}^{rex}(Y_{AE})$ are activation energy and entropy of the grain growth, respectively, M_0^{rex} is an empirical parameter, R_g is the gas constant. According to [23], activation entropy proportional to the corresponding energy will be treated with a fitting parameter β_{GG}, i.e. $S_{GG}(Y_{AE}) = \beta_{GG}\, Q_{GG}(Y_{AE})$.

The present model presumes that $Q_{GG}^{rex}(Y_{AE}) = \alpha_{GG}^{rex} Q_{SD}(Y_{AE})$, where $Q_{SD}(Y_{AE})$ is AESD in solid solution of complexly alloyed austenite and α_{GG}^{rex} is an empirical parameter. According to [22], the dependence of AESD on the chemical composition of the solid solution has the form:

$$\begin{aligned} Q_{SD}(Y_{AE}) = {} & 311691 - 278242\left(1-\exp(-0.394\, y_C)\right) + 88752\, y_{Mn}^{\,0.31} + 22801 y_{Si} - 6490\, y_{Cr} + \\ & 84864\, y_{Mo}^{\,0.65} - 38575\, y_{Ni}^{\,0.3} - 7298 y_V + 132594\, y_{Nb}^{\,0.263} + 82128\, y_{Ti}^{\,0.401} (J/mol). \end{aligned} \tag{15}$$

Recovery kinetics. The recovery responsible for material softening is ascribed first to gradual annihilation of dislocations, i.e. reduction of their density. This effect is expressed by [26,27]:

$$\frac{d\Delta\sigma(t)}{dt} = -\frac{64\Delta\sigma(t)^2 v_d}{9M^3\alpha_\rho^2 E(T)} \exp\left(-\frac{U_{rec}}{R_g T}\right) \sinh\left(\frac{\Delta\sigma(t) V_{rec}}{k_B T}\right), \tag{16}$$

where U_{rec} and V_{rec}, respectively, are activation energy and activation volume of the recovery process that are assumed to be equal 286 kJ/mol and $45b^3$ [13]; v_D is the Debye frequency set to be 2×10^{12} s^{-1}, $E(T) = 2.6\mu(T)$ is Young's modulus. To integrate Eq. (16), the initial condition

$$\Delta\sigma(t=0) = \sigma - \sigma_y, \tag{17}$$

is used, where σ is the deforming stress of austenite, dependent on temperature and plastic strain rate according to [19], and $\sigma_y \equiv \sigma_{0.2}$ is the yield stress of austenite similarly calculated at its plastic strain of 0.2%.

Note that previous expressions ignore the particle precipitations on dislocations of deformed austenite which hinders the dislocation slip and hence diminishes the softening. In order to allow for this important effect, Eq. (16) is modified [13]:

$$\left(\frac{d\Delta\sigma(t)}{dt}\right)_{eff} = \frac{d\Delta\sigma(t)}{dt}\left(1-\frac{N_p(t)}{N_n(t)}\right), \quad N_p < N_n$$
$$\left(\frac{d\Delta\sigma(t)}{dt}\right)_{eff} = 0, \quad N_p \geq N_n, \tag{18}$$

where $N_n(t)$ is the volume density of nodes of the current dislocation network and $N_p(t)$ is the total volume density of various particles precipitated at such nodes.

Precipitation of carbonitrides/carbides in deformed austenite. In addition to the above-considered recovery and recrystallization, the present integral model quantitatively describes precipitations on dislocations of deformed austenite. This treatment is based on classical equations for nucleation and growth of precipitate particles [28,29]. Specifically, we use an implementation of this approach developed in [13,25,30].

Nucleation of particles. According to the classical theory, stationary rate of nucleation is expressed as:

$$J_n = N_n Z \beta_c \exp\left(-\frac{\Delta G_c}{k_B T}\right), \tag{19}$$

where temperature and time dependencies of involved terms are omitted for brevity's sake. In this equation, N_n is the volume density of potential nucleation sites, Z is Zel'dovich factor admitting the fluctuation dissolution of supercritical embryos, β_c characterizes the rate of diffusion-controlled joining of Me atoms to an embryo of critical radius R_c, and k_B is Boltzmann's constant. The energy barrier for nucleation $\Delta G_c = \frac{4}{3}\pi R_c^2 \gamma_{p/\gamma}$ is conventionally expressed in terms of the specific interfacial energy $\gamma_{p/\gamma}$. Factor

$$\beta_c = \frac{4\pi R_c^2 D_{Me}^{v} X_{Me}}{a_\gamma^4}, \tag{20}$$

depends on the bulk diffusion coefficient D_{Me}^{v} of Me atoms dissolved in austenite and their molar fraction X_{Me}.

The critical size of an embryonic particle

$$R_c = -\frac{2\gamma_{p/\gamma}}{\Delta G_p^{Me(C,N);MeC}}, \tag{21}$$

is determined by the driving force $\Delta G_p^{Me(C,N);MeC}$ for its formation (considered below), and

$$Z = \left(\frac{\Delta G_c}{3\pi k_B T\, n_c^2}\right)^{1/2}, \tag{22}$$

involves the number $n_c = \frac{4}{3}\pi R_c^3 / V_a^{Me(C,N);MeC}$ of Me atoms in the critical embryo, where $V_a^{Me(C,N);MeC}$ is a volume per one Me atom in Me(C,N) or MeC particles.

The model considers particles that form at nodes of the dislocation network. As far as the number of free nodes is gradually diminished while the process develops, their time-dependent density takes on form:

$$N_n = N_n(t) = 0.5\,\alpha_N(t)\bar{\rho}_d^{1.5}(t), \tag{23}$$

where $\alpha_N(t)$ is the fraction of dislocation nodes which are not occupied by particles at time *t*.

Driving force of nucleation. Driving force $\Delta G_p^{Me(C,N)}$ for precipitation of Nb and V carbonitrides with various chemical compositions MeC_yN_{1-y} is expressed according to [30]:

$$\Delta G_p^{Me(C,N)} = -\frac{k_B T}{V_a^{Me(C,N)}} \ln\left[\frac{X_{Me}^{ss}(X_C^{ss})^y (X_N^{ss})^{1-y}}{(yK_{MeC})^y \left[(1-y)K_{MeN}\right]^{1-y}}\right], \tag{24}$$

where $X_{Me}^{ss}, X_C^{ss}, X_N^{ss}$ are molar fractions of the corresponding atoms dissolved in austenite, K_{MeC} and K_{MeN} are solubility products. The composition of critical embryos y_c [30] is assumed to provide the maximum magnitude of driving force (24) that means:

$$y_c = \left[1 + \frac{X_N^{ss}}{X_C^{ss}} \frac{K_{MeC}}{K_{MeN}}\right]^{-1}. \tag{25}$$

In the case of Ti carbides with solubility product K_{TiC} the precipitation driving force takes on a simpler form:

$$\Delta G_p^{TiC} = -\frac{k_B T}{V_a^{TiC}} \ln\left[\frac{X_{Ti}^{ss} X_C^{ss}}{K_{TiC}}\right]. \tag{26}$$

Based on the Thermo-Calc software package [31], we determine solubility products in (24)-(26) by the following equations:

$$\begin{aligned}
K_{NbC} &= \log[Nb][C] = 4.78 - \frac{10030 - 14.5[Mn] + 206.0[Si]}{T}, \\
K_{NbN} &= \log[Nb][N] = 4.37 - \frac{10780 - 35.3[Mn] + 225.6[Si]}{T}, \\
K_{VC} &= \log[V][C] = 6.72 - \frac{9500}{T}, \\
K_{VN} &= \log[V][N] = 4.57 - \frac{10290 - 56.5[Mn] + 255.4[Si]}{T}, \\
K_{TiC} &= \log[Ti][C] = 4.11 - \frac{9100 - 33.0[Mn] + 254.9[Si]}{T},
\end{aligned} \tag{27}$$

where [Nb], [V], [Ti] [C], [N], [Mn] and [Si] are mass fractions (%) of alloying elements in a solid solution.

Growth/dissolution rate. To follow the evolving particle radius, differential equation

$$\frac{dR}{dt} = \frac{D_{Me}^{eff}}{R} \frac{X_{Me}^{ss} - X_{Me}^{i}}{X_{Me}^{p} - X_{Me}^{i}}, \tag{28}$$

is applied, where D_{Me}^{eff} is the effective diffusion coefficient of Me atoms, X_{Me}^{p} is their concentration in particles and X_{Me}^{i} is their equilibrium concentration at the particle/matrix interface. According to [13,25], D_{Me}^{eff} is calculated with allowance for quick diffusion of these atoms along with dislocation cores:

$$D_{Me}^{eff} = \pi R_d^2 \overline{\rho}_d(t) D_{Me}^{d} + \left(1 - \pi R_d^2 \overline{\rho}_d(t)\right) D_{Me}^{v}, \tag{29}$$

where D_{Me}^{d} is the related diffusion coefficient and R_d is the radius of dislocation core, assumed to be 1.5*b*.

In the case of Nb and V carbonitrides which have various compositions, the interfacial concentrations are evaluated using simultaneous equations [30] for the balance and compatibility of diffusional fluxes:

$$
\begin{aligned}
&yK^{*}_{MeC} = X^{i}_{Me} X^{i}_{C},\\
&K^{*}_{MeN} = X^{i}_{Me} X^{i}_{N},\\
&D_C (X^{i}_{C} - X^{ss}_{C}) = yD_{Me} (X^{i}_{Me} - X^{ss}_{Me}),\\
&D_N (X^{i}_{N} - X^{ss}_{N}) = (1-y) D_{Me} (X^{i}_{Me} - X^{ss}_{Me}),
\end{aligned}
\tag{30}
$$

where $X^{i}_{C} = X^{i}_{C}(R)$, $X^{i}_{N} = X^{i}_{N}(R)$ are the interfacial concentrations of C and N, D_C, D_N are respective bulk diffusion coefficients in austenite, K^{*}_{MeC}, K^{*}_{MeN} are solubility products allowing for the Gibbs-Thompson effect:

$$
\begin{aligned}
&K^{*}_{MeC} = K_{MeC} \exp\left(\frac{2\gamma^{Me(C,N)}_{p/\gamma} V_a^{Me(C,N)}}{Rk_B T} \right),\\
&K^{*}_{MeN} = K_{MeN} \exp\left(\frac{2\gamma^{Me(C,N)}_{p/\gamma} V_a^{Me(C,N)}}{Rk_B T} \right),
\end{aligned}
\tag{31}
$$

$\gamma^{Me(C,N)}_{p/\gamma}$ is the specific energy of the particle-matrix interface.

Provided $D_C >> D_{Me}$ and $D_N >> D_{Me}$, equations (30) and (31) enable one to specify by the term y_g the current composition of the interfacial layer and determine the interfacial concentrations [30]:

$$
\begin{aligned}
&X^{i}_{Me} = \frac{K_{MeC} K_{MeN}}{K_{MeC} X^{ss}_{N} + K_{MeN} X^{ss}_{C}} \exp\left(\frac{2\gamma^{Me(C,N)}_{p/\gamma} V_a^{Me(C,N)}}{Rk_B T} \right),\\
&y_g = \left[1 + \frac{X^{ss}_{N}}{X^{ss}_{C}} \frac{K_{MeC}}{K_{MeN}} \right]^{-1}.
\end{aligned}
\tag{32}
$$

In the case of TiC particles which have a fixed composition, expression for interfacial concentrations takes on form:

$$
X^{i}_{Ti} = \frac{K_{TiC}}{X^{ss}_{C}} \exp\left(\frac{2\gamma^{TiC}_{p/\gamma} V_a^{TiC}}{Rk_B T} \right). \tag{33}
$$

The current concentration of alloying atoms in a solid solution. While the considered particles precipitate, quantities of alloying elements in the solid solution gradually diminish from initial values, dependent on the pre-treatment, to respective equilibrium levels at the reaction temperature. To save total quantities of alloying atoms when calculating of their concentrations both in particles and in the solid solution, the balance equation is applied:

$$
X^{p}_{Me} + X^{ss}_{Me} \left(1 - V_{Me(C,N);\,MeC} \right) = X^{0}_{Me}, \tag{34}
$$

where X^{0}_{Me} is the total molar concentration of Me atoms in steel and $V_{Me(C,N);\,MeC}$ are the current volume fractions of particles. According to this equation, concentrations of Nb, V, and Ti dissolved in austenite are expressed:

$$X_{Nb}^{ss} = \frac{X_{Nb}^{0} - X_{Nb}^{Nb(C,N)} V_{Nb(C,N)}}{1 - V_{Nb(C,N)}},$$
$$X_{V}^{ss} = \frac{X_{V}^{0} - X_{V}^{V(C,N)} V_{V(C,N)}}{1 - V_{V(C,N)}}, \quad (35)$$
$$X_{Ti}^{ss} = \frac{X_{Ti}^{0} - X_{Ti}^{TiC} V_{TiC}}{1 - V_{TiC}}.$$

Corresponding expressions for C and N have the form:

$$X_{N}^{ss} = \frac{X_{N}^{0} - X_{N}^{Nb(C,N)} V_{Nb(C,N)} (1 - \overline{y}_{Nb(C,N)}) - X_{N}^{V(C,N)} V_{V(C,N)} (1 - \overline{y}_{V(C,N)})}{1 - V_{Nb(C,N)} - V_{V(C,N)}},$$
$$X_{C}^{ss} = \frac{X_{C}^{0} - X_{C}^{Nb(C,N)} V_{Nb(C,N)} \overline{y}_{Nb(C,N)} - X_{C}^{V(C,N)} V_{V(C,N)} \overline{y}_{V(C,N)} - X_{C}^{TiC} V_{TiC}}{1 - V_{Nb(C,N)} - V_{V(C,N)} - V_{TiC}}, \quad (36)$$

where $\overline{y}_{Me(C,N)}$ is the average fraction of C atoms in Me(C,N) particles.

Sketch of modeling procedure for precipitation of particles. Following [29,30], we will use an incremental model that considers relatively small successive changes in short time steps $\delta t^{(k)}$. The particle size distribution function is upgraded at each step with allowance for both freshly appeared particles and the growth/dissolution of preexisting ones. Increment $J_n^{(k)} \delta t^{(k)}$ of the nascent particles number depends on nucleation rate $J_n^{(k)}$ at this step and, to upgrade the size distribution function, a new size class is created whose characteristic R_c^* slightly exceeds the previous R_c (see [30] for details):

$$R_c^* = R_c + \frac{1}{2} \sqrt{\frac{k_B T}{\pi \gamma_{p/\gamma}}}. \quad (37)$$

Characteristics y_c for particles of various composition is derived with equation (25) and their size in any *i*-th class (except for the nascent one) is increased by $\delta R_i^{(k)} = \frac{dR_i^{(k)}}{dt} \delta t^{(k)}$. The average composition of particles of this class on *k*-th time step is evaluated according to [30]:

$$y_i^{(k)} = y_i^{(k-1)} \left[1 - \frac{\left(R_i^{(k)}\right)^3 - \left(R_i^{(k-1)}\right)^3}{\left(R_i^{(k)}\right)^3} \right] + y_g \frac{\left(R_i^{(k)}\right)^3 - \left(R_i^{(k-1)}\right)^3}{\left(R_i^{(k)}\right)^3}, \quad (38)$$

where $y_i^{(k-1)}$ is the particle composition at time step (*k*-1), $R_i^{(k)}$ and $R_i^{(k-1)}$ are sizes for *i*-th class at time steps *k* and (*k*-1), respectively.

Then, based on predetermined size distribution function $N_{Me(C,N)}^{(i)}(R_{Me(C,N)}^{(i)})$, volume density $N_{Me(C,N)}$, average size $\overline{R}_{Me(C,N)}$, and volume fraction $V_{Me(C,N)}$ of Me(C,N) particles are calculated:

$$N_{Me(C,N)} = \sum_{i=1}^{n_{Me(C,N)}} N_{Me(C,N)}^{(i)},$$

$$\overline{R}_{Me(C,N)} = \frac{\sum_{i=1}^{n_{Me(C,N)}} N_{Me(C,N)}^{(i)} R_{Me(C,N)}^{(i)}}{N_{Me(C,N)}}, \tag{39}$$

$$V_{Me(C,N)} = \frac{4}{3}\pi \sum_{i=1}^{n_{Me(C,N)}} \left[N_{Me(C,N)}^{(i)} \left(R_{Me(C,N)}^{(i)} \right)^3 \right],$$

where $N_{Me(C,N)}^{(i)}$, $R_{Me(C,N)}^{(i)}$ are the volume density and radius of the considered particles in *i*-th class and $n_{Me(C,N)}$ is the number of classes in the distribution function. The average characteristic of variable particle composition is expressed by:

$$\overline{y}_{Me(C,N)} = \frac{\frac{4}{3}\pi \sum_{i=1}^{n_{Me(C,N)}} \left[N_{Me(C,N)}^{(i)} \left(R_{Me(C,N)}^{(i)} \right)^3 y_{Me(C,N)}^{(i)} \right]}{V_{Me(C,N)}}, \tag{40}$$

where $y_{Me(C,N)}^{(i)}$ specifies the composition of Me(C,N) particles in *i*-th class.

An important issue in the considered numerical procedure is the selection of time step. On the one hand, to ensure accuracy and convergence of the computational scheme, this step must be short enough; on the other hand, too small steps would suggest the inacceptable consumption of the computational power. For a reasonable compromise, the relative increments of concentration and volume fractions should not exceed 0.01. To comply with this restriction, the current time step is selected to be the least of:

$$\delta t_1^{(k)} = \frac{0.01 V_{Me(C,N)}^{(k)}}{\left| V_{Me(C,N)}^{(k)} - V_{Me(C,N)}^{(k-1)} \right|} \delta t^{(k-1)},$$

$$\delta t_2^{(k)} = \frac{0.01 X_{Me}^{ss\,(k)}}{\left| X_{Me}^{ss\,(k)} - X_{Me}^{ss\,(k-1)} \right|} \delta t^{(k-1)}. \tag{41}$$

3. Model calibration and discussion of modeling results

To simulate simultaneously the three interrelated processes (recovery, recrystallization, deformation-induced precipitation), empirical parameters of the model have been determined in two steps. First, recrystallization parameters allowing for the concurrent recovery are found while assuming that atoms of all alloying elements including MAE are completely dissolved in austenite, i.e. no precipitation takes place. Next, additional parameters, needful to model the precipitation kinetics and interaction of nascent particles with boundaries of recrystallized grains, are obtained. All the parameters are fitted to wide experimental data on austenite recrystallization in a wide range (23 steels) of chemical composition listed in Table 1. Details of the calibration procedure are described in what follows.

Recrystallization and recovery. To determine an important parameter α_{rex}^{*}, Eq. (12) for the recrystallized grain size has been fitted to experimental data on steels S0 [7] and S00 [17]. The resulting $\alpha_{rex}^{*} = 8.6 \times 10^{-4}\,\mathrm{m^2 N^{-2}}$ satisfactorily comply with these data covering practically significant ranges of temperature and strain degree of austenite, as well as initial grain sizes (Fig. 1). Other parameters have been fitted to wide data on austenite recrystallization

in steels S1-S10 at relatively high temperatures where atoms of all alloying elements are in solid solution.

Table 1. Chemical composition (mass.%) of steels employed in model calibration

Steel	C	Mn	Si	Cr	Ni	Mo	Nb	V	Ti	N	Ref.
S0	0.17	0.74	0.01	–	–	–	–	–	–	–	[7]
S00	0.05	1.88	0.04	–	–	0.49	0.048	–	–	–	[17]
S1	0.11	0.55	0.26	–	–	–	–	–	–	–	[1-4, 6,8]
S2	0.53	0.71	0.21	–	–	–	–	–	–	–	
S3	0.42	0.79	0.27	–	–	0.18	–	–	–	–	
S4	0.44	0.79	0.23	–	–	0.38	–	–	–	–	
S5	0.11	1.32	0.24	–	–	–	0.070	–	–	–	
S6	0.12	1.10	0.24	–	–	–	–	0.07	–	–	
S7	0.15	1.25	0.27	–	–	–	–	–	0.017	–	
S8	0.08	1.47	0.20	–	–	0.19	0.042	0.06	0.010	0.006	Own results
S9	0.04	1.90	0.25	0.11	0.45	0.31	0.051	0.02	0.020	0.005	
S10	0.11	0.36	0.23	0.39	1.91	0.31	0.011	0.01	–	–	
S11	0.11	1.23	0.24	–	–	–	0.041	–	–	0.0112	[1-4, 6,8]
S12	0.11	1.32	0.24	–	–	–	0.093	–	–	0.0119	
S13	0.21	1.08	0.18	–	–	–	0.024	–	–	0.0058	
S14	0.21	1.14	0.19	–	–	–	0.058	–	–	0.0061	
S15	0.11	1.10	0.24	–	–	–	–	0.043	–	0.0105	
S16	0.12	1.10	0.24	–	–	–	–	0.060	–	0.0123	
S17	0.11	1.05	0.24	–	–	–	–	0.093	–	0.0144	
S18	0.21	1.10	0.20	–	–	–	–	0.062	–	0.0134	
S19	0.15	1.25	0.27	–	–	–	–	–	0.055 **0.021***	–	
S20	0.15	1.10	0.26	–	–	–	–	–	0.075 **0.040***	–	
S21	0.06	1.70	0.20	–	–	0.20	0.045	0.040	0.020	0.005	Own results

*Contents obtained by taking into account Ti binding in TiN particles.

Thus obtained $\alpha_{d1} = 0.2$ and $\alpha_{d2} = 2.2$ for Eq. (6) suggest that the driving pressure near grain boundaries at the beginning of recrystallization ($X(t=0)=0$) corresponds to the dislocation density $\rho_d(t=0) = 1.2\overline{\rho}_d(t=0)$ whereas $\rho_d(t) = 0.3\overline{\rho}_d(t)$ when the process completes ($X(t)=1$). Parameters of Eq. (15) for the boundary mobility are $\alpha_{GG}^{rex} = 0.64$, $\beta_{GG}^{rex} = 5.21\times10^{-5}\,\mathrm{K}^{-1}$ and $M_0 = 6.5\times10^{-10}\,\mathrm{m^3 s^{-1} N^{-1}}$.

Kinetics of austenite recrystallization in steels S1-S10, simulated with allowance for recovery, as well as corresponding experimental data are represented in Fig. 2a-l evidencing that derived parameters provide good prediction power of the model in a wide range of temperature (900÷1150ºC), chemical composition (Table 1), initial grain size (30÷205 μm) and deformation conditions (ε=0.2÷0.35; $d\varepsilon/dt$=0.5÷5 s^{-1}). The average relative error of the predicted recrystallization degree (volume fraction) does not exceed 13% (Fig. 2m).

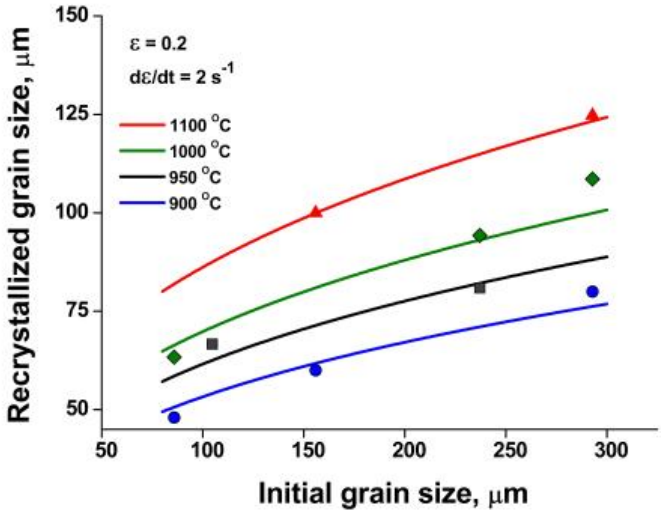

Fig. 1. Comparison of the calculated size of recrystallized grain (lines) with experimental data (symbols) for S0 steel [7]

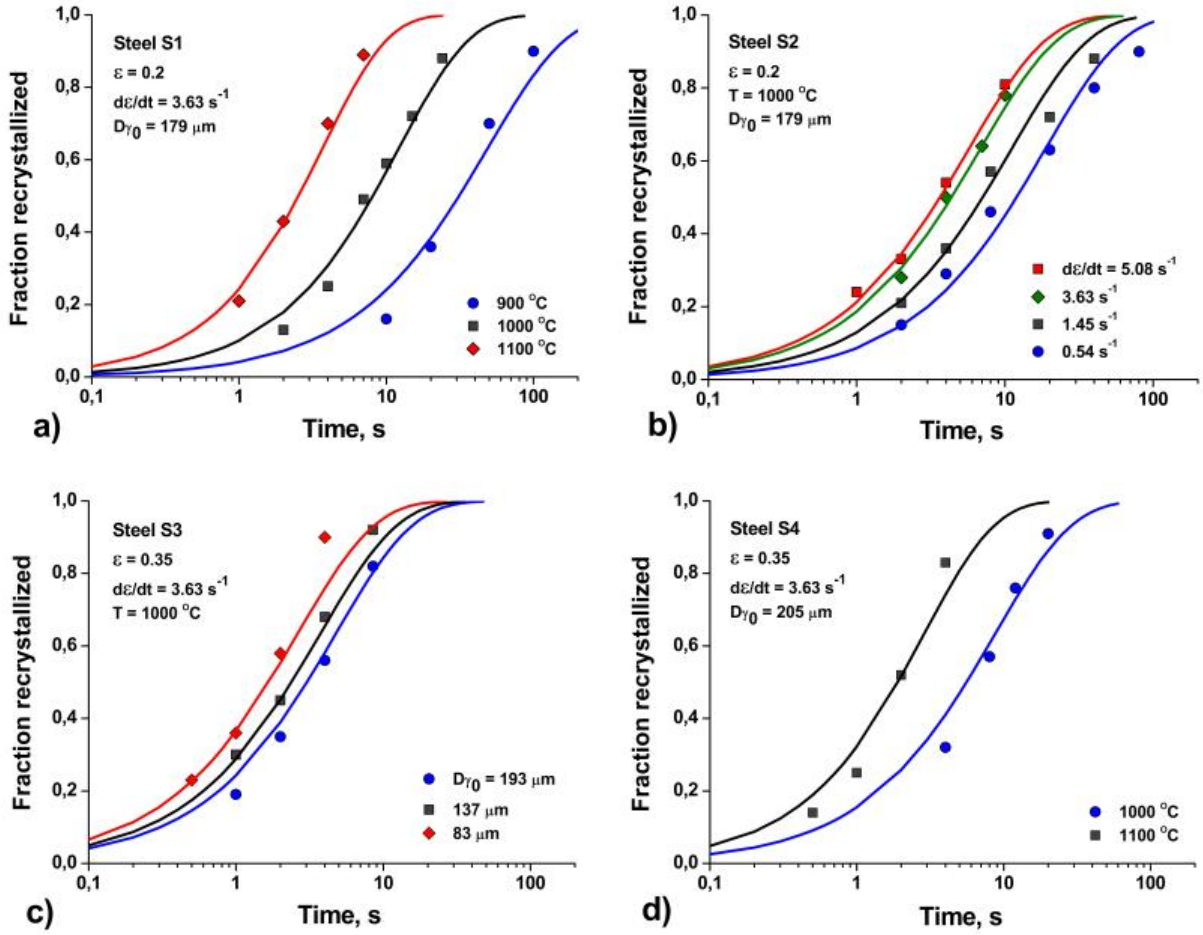

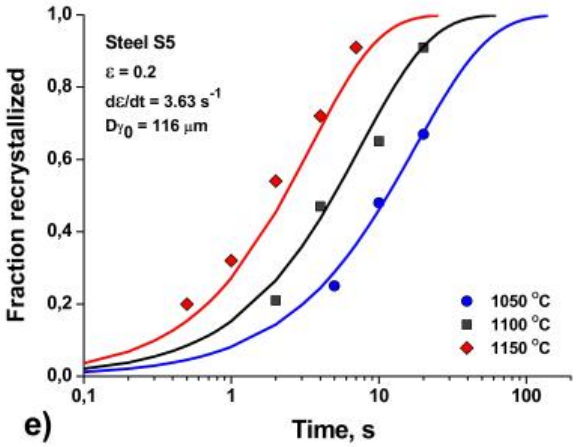
Steel S5
ε = 0.2
dε/dt = 3.63 s-1
Dγ0 = 116 μm
1050 °C
1100 °C
1150 °C
Fraction recrystallized
Time, s
e)

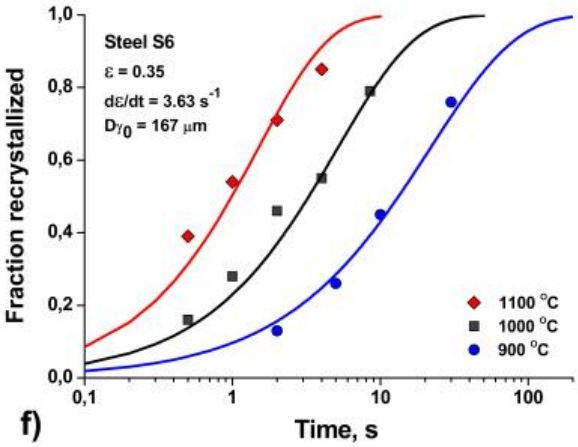
Steel S6
ε = 0.35
dε/dt = 3.63 s-1
Dγ0 = 167 μm
1100 °C
1000 °C
900 °C
Fraction recrystallized
Time, s
f)

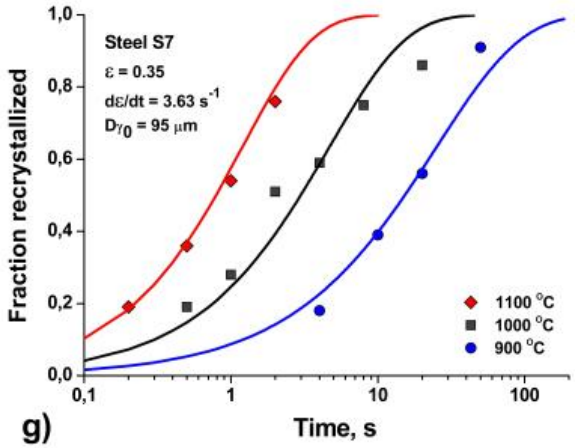
Steel S7
ε = 0.35
dε/dt = 3.63 s-1
Dγ0 = 95 μm
1100 °C
1000 °C
900 °C
Fraction recrystallized
Time, s
g)

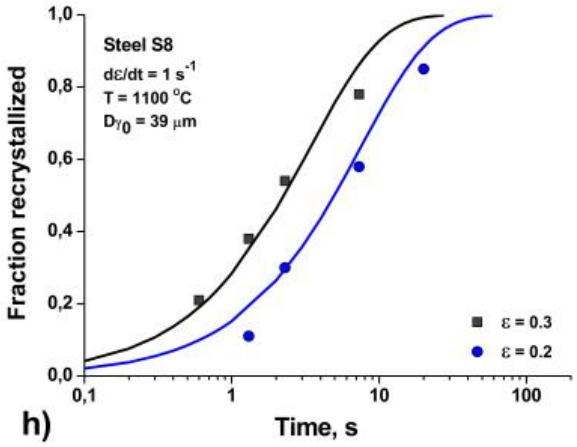
Steel S8
dε/dt = 1 s-1
T = 1100 °C
Dγ0 = 39 μm
ε = 0.3
ε = 0.2
Fraction recrystallized
Time, s
h)

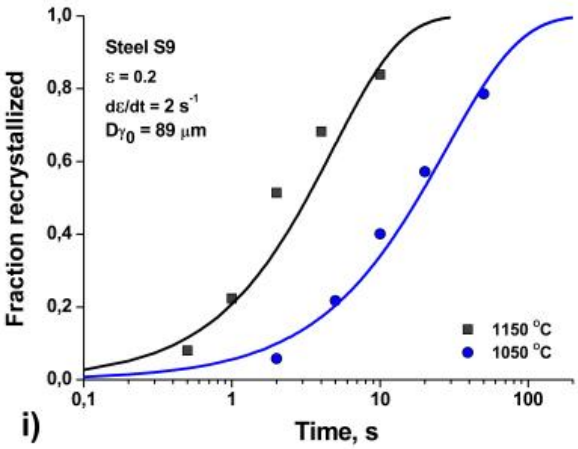
Steel S9
ε = 0.2
dε/dt = 2 s-1
Dγ0 = 89 μm
1150 °C
1050 °C
Fraction recrystallized
Time, s
i)

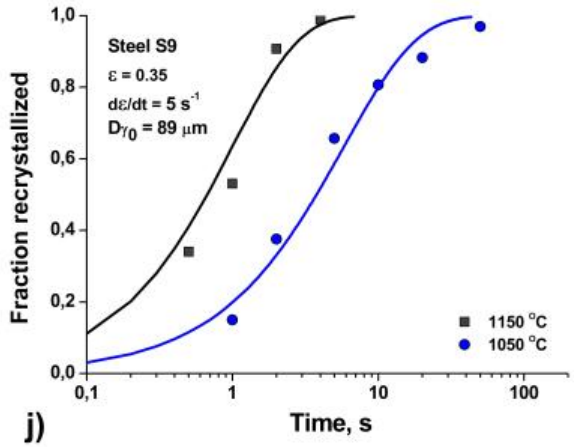
Steel S9
ε = 0.35
dε/dt = 5 s-1
Dγ0 = 89 μm
1150 °C
1050 °C
Fraction recrystallized
Time, s
j)

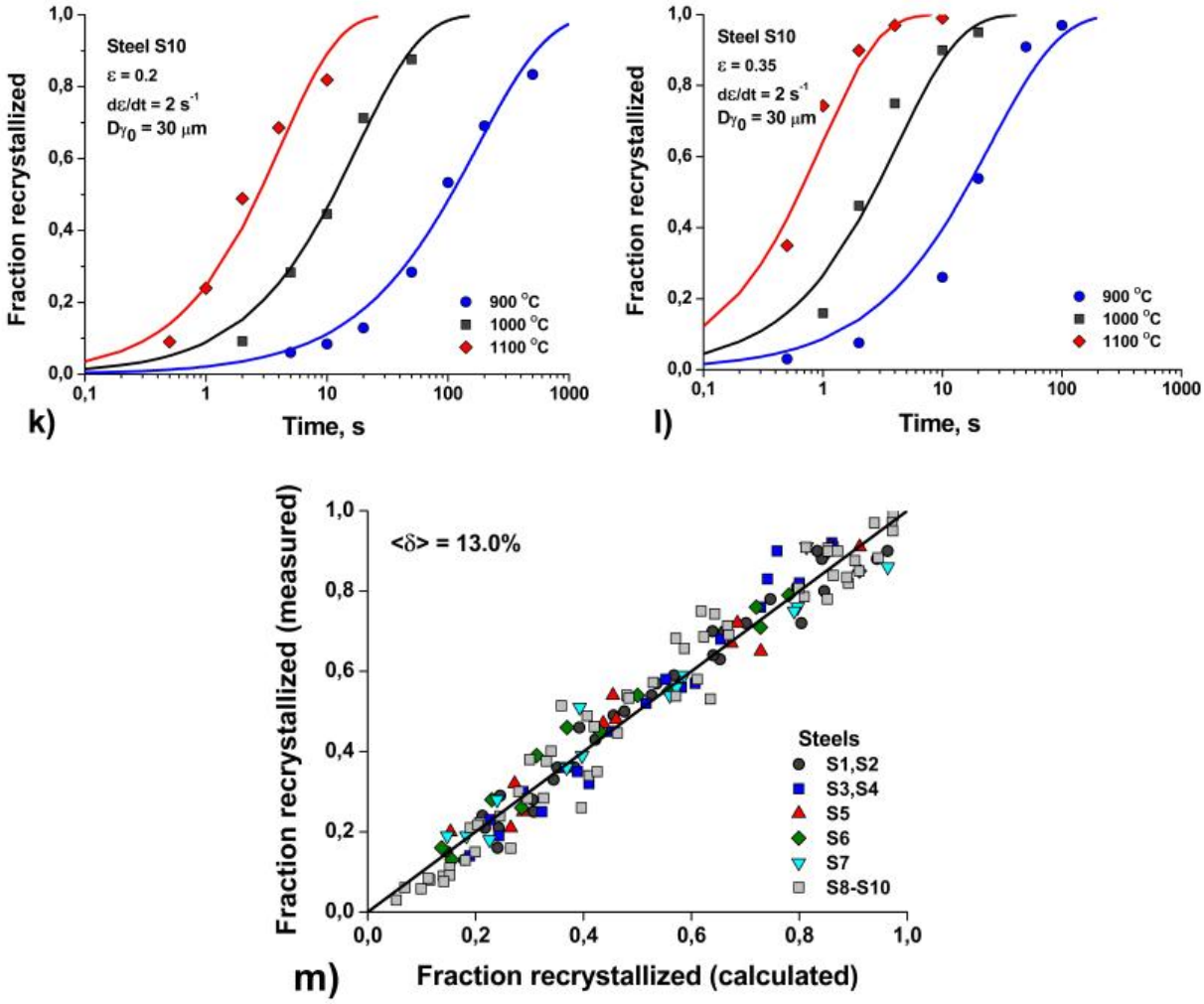

Fig. 2. Comparison of simulated recrystallization kinetic curves (a-l) for steels S1-S10 at different temperatures, sizes of the initial austenite grain ($D_{\gamma 0}$) and deformation parameters (ε, dε/dt) to experimental data (symbols), and comparison of model predictions to actual recrystallized fractions (m) (<δ> is a magnitude of the average relative error)

Note that obtained $\alpha_{GG}^{rex} = 0.64$ confirms, as expected, that effective activation energy $Q_{GG}^{rex}(Y_{AE})$ for migration of recrystallized grain boundaries is comparable to that for the grain boundary self-diffusion. The range of chemical composition where the model displays good performance corresponds to a significant variation of $Q_{GG}^{rex}(Y_{AE})$ between 146.1 kJ/mol (S2) and 308.1 kJ/mol (S9). It is remarkable as well that the considered activation energy suggests a novel approach to the grain boundary mobility depending on the chemical composition of austenite solid solution. Specifically, unlike the classical model of "solute drag effect" [32] or the later "statistical solute-pinning theory" [33,34], the present model enables reasonable predictions with no explicit allowance for any pinning by solute atoms. This is rather surprising insofar as the considered steels contain high amounts of Mn, Mo, and Nb to which the solute drag is commonly ascribed.

Deformation induced precipitation of particles. This step of calibration determines specific energies of particle boundaries $\gamma_{Nb(C,N)/\gamma}$, $\gamma_{V(C,N)/\gamma}$ and $\gamma_{TiC/\gamma}$ as well as specific energy γ_{GB} of recrystallized grain boundaries. To simulate precipitation processes, diffusion coefficients of Me atoms should also be employed. Such terms for the bulk diffusion of various

MAE have been found in the literature (Table 2). To evaluate coefficients of the dislocation "pipe" diffusion absent in the literature, related activation energies have been assumed to be halves of their bulk counterparts (Table 2).

Table 2. Model parameters for precipitation of various particles

Parameter	Values
Volume per atom of Me in a particle, m^3	$V_a^{Nb(C,N)} = 2.22\times10^{-29}$ $V_a^{V(C,N)} = 1.75\times10^{-29}$ [35] $V_a^{TiC} = 2.04\times10^{-29}$
Bulk diffusion coefficient of Me atoms, m^2s^{-1}	$D_{Nb}^{v} = 0.83\times10^{-4}\exp(-266500/R_gT)$ [13] $D_{V}^{v} = 0.25\times10^{-4}\exp(-264200/R_gT)$ [30] $D_{Ti}^{v} = 0.15\times10^{-4}\exp(-251200/R_gT)$ [36]
Dislocation pipe diffusion coefficients of Me atoms, m^2s^{-1}	$D_{Nb}^{d} = 0.83\times10^{-4}\exp(-133250/R_gT)$ $D_{V}^{d} = 0.25\times10^{-4}\exp(-132100/R_gT)$ $D_{Ti}^{d} = 0.15\times10^{-4}\exp(-125600/R_gT)$
Specific energy of particle/matrix interface, J/m^2	$\gamma_{Nb(C,N)/\gamma} = 0.26 - 0.095\exp(-5410y_{Nb})$ $\gamma_{V(C,N)/\gamma} = 0.35 - 0.129\exp(-2840y_{V})$ $\gamma_{TiC/\gamma} = 0.33$

In fitting $\gamma_{Nb(C,N)/\gamma}$ to data on recrystallization kinetics of steels S11-S14 micro-alloyed by Nb under the solvus temperature of Nb(C,N), a significant effect of its reduction when increasing quantity of Nb in steel has been revealed. The corresponding dependence of $\gamma_{Nb(C,N)/\gamma}$ on y_{Nb} is evident in Table 2. The latter shows as well that a similar effect derived from data on steels S15−S18 is peculiar to $\gamma_{V(C,N)/\gamma}$. At the same time, the recrystallization kinetics of steels S19 and S20 micro-alloyed by Ti does not display a certain dependence of $\gamma_{TiC/\gamma}$ on Ti content under the solvus temperature of TiC. When such particles precipitate, the process kinetics is satisfactorily described with constant $\gamma_{TiC/\gamma}$.

The monotonous diminishing of effective γ_{GB} at increasing temperature, revealed in calibrating the integral model, is satisfactorily approximated by $\gamma_{GB}(T) = 2.46\times10^{7}\exp(-0.014T)$ J/mol. Qualitatively similar temperature dependence of γ_{GB} was obtained in [13].

Figure 3 illustrates the correspondence of modeling results, obtained with the above-considered empirical parameters, to experimental data on recrystallization kinetics in various micro-alloyed steels. Apparently, the model has good performance in application to both steels micro-alloyed by one of Nb, V, Ti (Fig. 3a,b; 3c,d, and 3e, respectively) and complexly micro-alloyed steels (Fig. 3f).

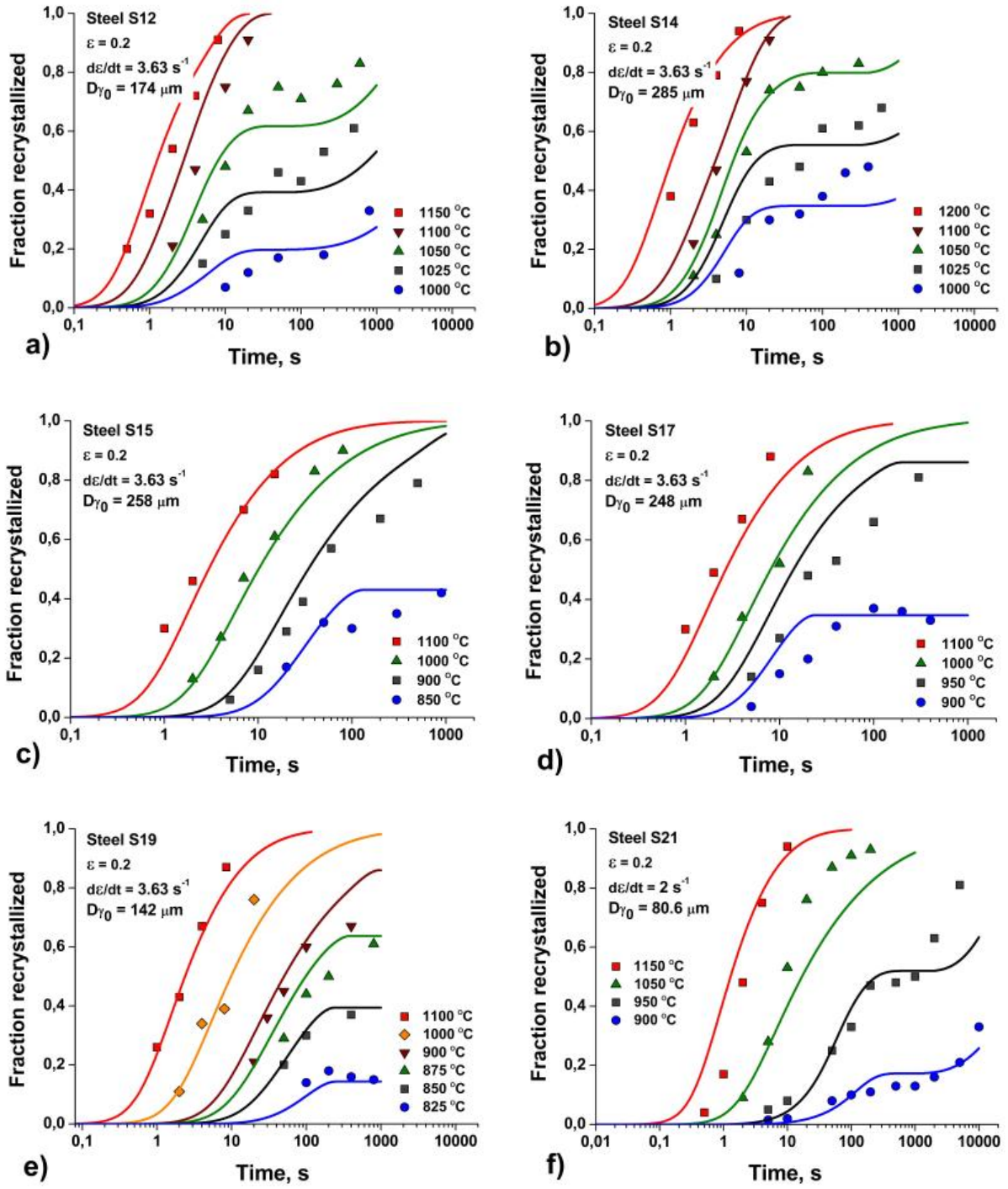

Fig. 3. Comparison of modeling results of recrystallization kinetic curves for steels S13-S18 (a-f) at different temperatures, sizes of the initial austenite grains ($D_{\gamma 0}$) and deformation parameters (ε, dε/dt) with experimental data (symbols)

4. Conclusions

A physically motivated model is formulated to predict the static recrystallization kinetics of austenite and the resulting grain size in complexly alloyed steels including those micro-alloyed by Nb, V, and Ti. The model simultaneously treats the three interrelated phenomena of recrystallization, recovery, and the deformation-induced precipitations. It is presumed that activation energy of the process is proportional to the activation energy of bulk self-diffusion,

the latter being dependent on the chemical composition of the solid solution according to the previously established empirical expression.

Empirical parameters of the model were fitted to an extensive database on the kinetics of austenite recrystallization for 23 steels with a wide range of chemical composition (mass.%): C (0.04÷0.53), Mn (0.36÷1.90), Si (0.01÷0.27), Cr (0.11÷0.39), Ni (0.45÷1.91), Mo (0.18÷0.49), Nb (0.00÷0.093), V (0.00÷0.093), Ti (0.00÷0.075). The fitting is implemented in two steps as follows. The first step, using relevant data on 12 steels, determines recrystallization parameters with allowance for the recovery effect in the case of complete dissolution of alloying elements including microalloying ones, i.e. when no precipitation takes place. Kinetic parameters of particles precipitation on dislocations of deformed austenite, as well as their interaction with migrating boundaries of recrystallized grains, are derived from experimental data on 11 micro-alloyed steels.

As shown in this work, the proposed model of austenite recrystallization complies well with experiments on numerous steels in a wide range of temperature (825÷1200ºC), initial grain size (30÷285 μm), the degree (0.2÷0.35) and rate (0.5÷5 s^{-1}) of strain. The process activation energy in the considered wide range of chemical compositions varies by more than two times (146.1 to 308.1 kJ/mol). An interesting property of the model is that good correspondence to experimental data is achieved with no explicit allowance for the boundary pinning by dissolved Me atoms although the treated steels contain Mn, Mo, and Nb to which the pronounced solute drag effect is commonly ascribed.

Acknowledgments. *This work was supported by the grant from the Russian Science Foundation (project No. 19-19-00281).*
The authors are grateful to Prof. Alexander Zisman for useful discussions of the work.

References

[1] Medina SF, Mancilla JE, Hernandez CA. Static recrystallization of hot deformed austenite and induced precipitation kinetics in vanadium micro-alloyed steels. *Iron and Steel Institute of Japan International*. 1994;34(8): 689-696.
[2] Medina SF, Mancilla JE. Influence of alloying elements in solution on static recrystallization kinetics of hot deformed steels. *Iron and Steel Institute of Japan International*. 1996;36(8): 1063-1069.
[3] Medina SF, Mancilla JE. Static recrystallization modelling of hot deformed steels containing several alloying elements. *Iron and Steel Institute of Japan International*. 1996;36(8): 1070-1076.
[4] Medina SF, Quispe A. Influence of strain on induced precipitation kinetics in micro-alloyed steels. *Iron and Steel Institute of Japan International*. 1996;36(10): 1295-1300.
[5] Li G, Maccagno TM, Bai DQ, Jonas JJ. Effect of initial grain size on the static recrystallization kinetics of Nb micro-alloyed steels. *Iron and Steel Institute of Japan International*. 1996;36(12): 1479-1485.
[6] Quispe A, Medina SF, Valles P. Recrystallization-induced precipitation interaction in a medium carbon vanadium micro-alloyed steel. *Iron and Steel Institute of Japan International*. 1997;37(8): 783-788.
[7] Sun WP, Militzer M, Hawbolt EB, Meadowcroft TR. Austenite grain refinement and growth during the thermomechanical processing of steels. In: Chandra T. (ed.) *Thermec'97*. Warrendale: TMS; 1997. p.685-691.
[8] Medina SF, Quispe A, Valles P, Banos JL. Recrystallization-precipitation interaction study of two medium carbon niobium micro-alloyed steels. *Iron and Steel Institute of Japan International*. 1999;39(9): 913-922.

[9] Cho S, Kang K, Jonas JJ. The dynamic, static and metadynamic recrystalliztion of a Nb-microalloyed steel. *Iron and Steel Institute of Japan International*. 2000;36(9): 914-921.
[10] Cho S, Kang K, Jonas JJ. Mathematical modelling of the recrystallization kinetics of Nb microalloyed steels. *Iron and Steel Institute of Japan International*. 2001;41(7): 766-773.
[11] Medina HS, Quispe A. Improved model for static recrystallization kinetics of hot deformed austenite in low alloy and Nb/V micro-alloyed steels. *Iron and Steel Institute of Japan International*. 2001;41(7): 774-781.
[12] Zurob HS, Hutchison CR, Brechet Y, Purdy G. A model for the competition of precipitation and recrystallization in deformed austenite. *Acta Materialia*. 2001;49(20): 4183-4190.
[13] Zurob HS, Hutchison CR, Brechet Y, Purdy G. Modelling recrystallization of microalloyed austenite: effect of coupling recovery, precipitation and recrystallization. *Acta Materialia*. 2002;50(12): 3075-3092.
[14] Gomez M, Medina SF, Quispe A, Valles P. Static recrystallization and induced precipitation interaction in a low Nb micro-alloyed steels. *Iron and Steel Institute of Japan International*. 2002;42(4): 423-431.
[15] Zurob HS, Subramanian SV, Purdy G, Hutchison CR, Brechet Y. Analysis of the effect of Mn on the recrystallization kinetics of high Nb steel: An example of physically-based alloy design. *Iron and Steel Institute of Japan International*. 2005;45(5): 713-722.
[16] Quispe A, Medina SF, Gomezic M, Chaves JI. Influence of austenite grain size on recrystallization-precipitation interaction in a V-microalloyed steel. *Materials Science and Engineering A*. 2007;447(1-2): 11-18.
[17] Sarkar S, Moreau A, Militzer M, Poole WJ. Evolution of austenite recrystallization and grain growth using laser ultrasonics. *Metallurgical and Materials Transactions A*. 2008;39A: 897-907.
[18] Gomez M, Rancel L, Medina SF. Effect of aluminium and nitrogen on static recrystallization in V-microalloyed steels. *Materials Science and Engineering A*. 2009;506(1-2): 165-173.
[19] Vasilyev A, Rudskoy A, Kolbasnikov N, Sokolov S, Sokolov D. Physical and mathematical modeling of austenite microstructure evolution processes developing in line-pipe steels under hot rolling. *Material Science Forum*. 2012;706-709: 2836-2841.
[20] Kubota M, Kobayashi Y, Ushioda K, Takahashi J. Effect of carbon content on static recrystallization behavior of work-hardened austenite in low alloy steel and its mechanism. *Materials Transactions*. 2017;58(2): 196-205.
[21] Verhoeven JD. *Fundamentals of physical metallurgy*. John Wiley & Sons; 1975.
[22] Vasilyev AA, Sokolov SF, Kolbasnikov NG, Sokolov DF. Effect of alloying on the self-diffusion activation energy in γ-iron. *Physics of the solid state*. 2011;53(11): 2194-2200.
[23] Vasilyev AA, Sokolov SF, Sokolov DF, Kolbasnikov NG. Modeling of grain growth kinetics in complexly alloyed austenite. *Letters on Materials*. 2019;9(4): 419-423.
[24] Lefevre-Schlick F, Brechet Y, Zurob HS, Purdy G, Embury D. On the activation of recrystallization nucleation sites in Cu and Fe. *Mater. Sci. Eng. A*. 2009;502(1-2): 70-78.
[25] Dutta B, Palmiere EJ, Sellars CM. Modelling the kinetics of strain induced precipitation in Nb microalloyed steels. *Acta Materialia*. 2001;49(5): 785-794.
[26] Verdier M, Brechet Y, Guyot P. Recovery of AlMg alloys: flow stress and strain-hardening properties. *Acta Materialia*. 1999;47(1): 127-134.
[27] Smith A, Luo H, Hanlon DN, Sietsma J, Zwaag S. Recovery processes in the ferrite phase in C-Mn steel. *Iron and Steel Institute of Japan International*. 2004;44(7): 1188-1194.
[28] Wagner R, Kampmann R, Voorhees PW. *Homogeneous second-phase precipitation*. In: Kostorz G. (ed.) *Phase transformations in materials*. Weinheim: WILEY-VCH Verlag GmbH; 2001. p.309-407.

[29] Perez M, Dumont N, Acevedo-Reyes D. Implementation of classical nucleation and growth theories for precipitation. *Acta Materialia*. 2008;56: 2119-2132.
[30] Maugis P, Goune M. Kinetics of vanadium carbonitride precipitation in steel: A computer model. *Acta Materialia*. 2005;53: 3359-3367.
[31] Thermo-Calc Software: http://www.thermocalc.com
[32] Cahn JW. The impurity-drag effect in grain boundary motion. *Acta Metall*. 1962;10(9): 789-798.
[33] Hersent E, Marthinsen K, Nes E. The effect of solute atoms on grain boundary migration: A solute pinning approach. *Metallurgical and Materials Transactions A*. 2013;44(7): 3364-3375.
[34] Hersent E, Marthinsen K, Nes E. A solute pinning approach to solute drag in multi-component solid solution alloys. *Modeling and Numerical Simulation of Material Science*. 2014:4(1): 8-14.
[35] Gladman T. *The physical metallurgy of microalloyed steels*. Institute of materials; 1997.
[36] Liu WJ, Jonas JJ. Nucleation kinetics of Ti carbonitride in microalloyed austenite. *Metallurgical and Materials Transactions A*. 1989;20(4): 689-697.